Fabrication of concave micromirrors for single cell imaging *via* controlled over-exposure of organically modified ceramics in single step lithography

A. Bonabi,[1] S. Cito,[1,a)] P. Tammela,[2] V. Jokinen,[3] and T. Sikanen[1,b)]
[1]*Division of Pharmaceutical Chemistry and Technology, Faculty of Pharmacy, University of Helsinki, Helsinki, Finland*
[2]*Division of Pharmaceutical Biosciences, Faculty of Pharmacy, University of Helsinki, Helsinki, Finland*
[3]*Department of Materials Science and Engineering, School of Chemical Technology, Aalto University, Espoo, Finland*

(Received 2 March 2017; accepted 31 May 2017; published online 12 June 2017)

This work describes the fabrication of concave micromirrors to improve the sensitivity of fluorescence imaging, for instance, in single cell analysis. A new approach to fabrication of tunable round (concave) cross-sectional shaped microchannels out of the inorganic-organic hybrid polymer, Ormocomp®, *via* single step optical lithography was developed and validated. The concave micromirrors were implemented by depositing and patterning thin films of aluminum on top of the concave microchannels. The round cross-sectional shape was due to residual layer formation, which is inherent to Ormocomp® upon UV exposure in the proximity mode. We show that it is possible to control the residual layer thickness and thus the curved shape of the microchannel cross-sectional profile and eventually the focal length of the micromirror, by simply adjusting the UV exposure dose and the distance of the proximity gap (to the photomask). In general, an increase in the exposure dose or in the distance of the proximity gap results in a thicker residual layer and thus an increase in the radius of the microchannel curvature. Under constant exposure conditions, the radius of curvature is almost linearly dependent on the microchannel aspect ratio, i.e., the width (here, 20–200 μm) and the depth (here, 15–45 μm). Depending on the focal length, up to 8-fold signal enhancement over uncoated, round Ormocomp® microchannels was achieved in single cell imaging with the help of the converging micromirrors in an epifluorescence microscopy configuration. *Published by AIP Publishing*. [http://dx.doi.org/10.1063/1.4985653]

I. INTRODUCTION

The sensitivity of optical detection is an acknowledged challenge in chemical and biological microfluidics. Upon miniaturization, the optical path length is unavoidably decreased and this needs to be compensated by adding integrated optical elements, such as planar, polymer-based or tunable, liquid-based microlenses or microlens arrays for beam focusing.[1] Micromirrors and planar optical waveguides have also been implemented on microfluidic devices for beam steering purposes.[1] Although modern fluorescence-based techniques provide selective monitoring of fluorescent-derivatized biomolecules at sufficiently low levels also on microfluidic devices, there is a constant demand for new approaches that would allow ever better detection sensitivity. Particularly useful are such approaches that are compatible with the common optical microscopic settings and do not significantly increase the complexity of microfabrication or device operation. The present work addresses these needs by demonstrating a simple microfabrication approach

[a)]Present address: Department of Mechanical Engineering, Rovira i Virgili University, Tarragona, Spain
[b)]Author to whom correspondence should be addressed: tiina.sikanen@helsinki.fi. Tel.: +358-294159173.

that results in concave micromirrors with tunable focal length and fully integrated with in-channel microfluidics for fluorescence microscopy applications. Thanks to their concave shape, the micromirrors simultaneously improve the detection sensitivity *via* reflection and beam focusing. Most importantly, the chosen microfabrication material is feasible for standard lithographic processing and as such inherently bio- and cell-compatible.

Lithographic processing generally allows for total control over the shape of the patterns in the projected (horizontal) plane, but the possibilities to customize the microchannel cross-sectional shape in the vertical direction are limited.[2] Particularly, the fabrication of microchannels with a round cross-sectional shape in a controlled and tunable manner remains challenging. Most microfabrication processes and materials result in vertical or tilted microchannel walls, including direct lithography (of, e.g., SU-8), deep reactive ion etching, and anisotropic wet etching of silicon.[2] Few methods are available for fabrication of curved cross sections. Isotropic etching of glass produces rounded cross sections, but the process is inherently limited in the achievable shapes due to the way the feature size and the depth are interconnected.[2] Photoresist melting (reflow) produces spherical shapes, but the exact curvatures are difficult to control and only convex structures can be directly produced (although these can be replicated into concave structures during downstream processes).[3] Similar considerations apply to other approaches where liquid droplets are used, such as ink-jet printing (of microlenses).[4] Although direct ink-jet imprinting of concave polydimethylsiloxane (PDMS) structures[5] and restructuring of polystyrene into concave microlens arrays by an ink-jetting solvent (toluene) on a flat polymer surface[6] have been demonstrated, these approaches hardly allow the tunable cross-sectional shape. The emerging 3D printing techniques[7,8] are also capable of creating rounded grooves, but the resulting surfaces are rough and suffer from non-uniformity, which limits the use of 3D printed microstructures in optical settings where smooth surfaces are required to minimize optical losses at the interfaces. Also the feature resolution in 3D printing is typically in the range of tens to hundreds micrometers at best[7,8] and thus far from lithographic accuracy.

In this work, we describe fabrication of microchannels with a tunable, round (concave) cross-sectional shape out of organically modified ceramics (ORMOCER®s) in a controlled, yet rapid manner *via* single step lithography. ORMOCER®s are a new class of inorganic-organic hybrid polymers, which enable fast and simple microfabrication by UV-lithography and hold glass-like material properties after curing.[9,10] Beside lithography, ORMOCER®s can also be patterned by UV embossing,[10] direct laser writing,[11] and ink-jet printing.[12] Thanks to their good biocompatibility, ORMOCER®s are ideal for a variety of bioanalytical[10,13,14] and biomedical applications, including cell culturing[15,16] and cell migration assays,[17] tissue engineering,[18] and dentistry.[19] A range of different ORMOCER® materials is also available for antiadhesive and antistatic coatings[20] and optical waveguiding.[21] One of the commercial ORMOCER® formulations, Ormocomp®, has recently been introduced to fabrication of microchannels for capillary electrophoresis[13] and electrospray ionization microchips.[14] Surfaces with controlled porosity,[22] sample plates for laser desorption ionization mass spectrometry,[23] and nanopillar surfaces for fluidics and mass spectrometry[24] have also been implemented on Ormocomp®.

Since Ormocomp® is in a liquid form prior to UV exposure, the lithographic patterning must be done in the proximity (non-contact) exposure mode, which gives rise to diffraction of light below the photomask. Under these conditions, the high sensitivity of Ormocomp® to UV light results in overexposure and formation of a round (concave) shape with a residual layer that can extend tens of micrometers or more under the masked areas.[10] Thus, the profile of overexposed Ormocomp® is different from the typical negative profile of negative resists, such as that of SU-8.[25] Instead, the overexposed Ormocomp® profile more resembles the residual layer commonly formed during embossing processes (between the stamp and the substrate). From the microfabrication viewpoint, the residual layer is usually considered to have a negative impact on the resulting microstructures, but in this work, we take advantage of it and show that by adjusting the UV exposure dose or the distance of the proximity gap, the residual layer (here, defined as the difference between the nominal layer thickness and measured height) can be exploited to fabrication of round (concave) cross-sectional shaped microchannels in a controlled and tunable manner. In addition to UV curing conditions, the effect of the channel

aspect ratio on the obtained (concave) shape of the microchannel is demonstrated. Finally, to obtain the concave micromirrors, we pattern thin-film (100 nm) aluminum elements on top of the Ormocomp® microchannels. The inherent high surface smoothness of lithographically defined Ormocomp® plays a key role in facilitating elimination of optical losses at interfaces and thus implementation of high quality concave micromirrors with tunable focal length (as a result of the tunable microchannel radius of curvature) for single cell imaging by epifluorescence microscopy.

II. EXPERIMENTAL

A. Materials and reagents

Ormocomp® and OrmoDev® developer were purchased from Microresist Technology Gmbh (Berlin, Germany). Poly(dimethyl siloxane) (PDMS) was prepared from the Sylgard 184 base elastomer and the curing agent (Down Corning Corporation, Midland, MI). Fluorescein sodium salt was purchased from Sigma Aldrich (Steinheim, Germany) and sodium hydroxide and boric acid were purchased from Riedel-de Haën (Seelze, Germany). Water was purified with a Milli-Q water purification system (Millipore, Molsheim, France).

Baby hamster kidney (BHK-21) cell line transfected with non-cytotoxic Chikungunya virus replicon (CHIKV-NCT) containing the virus replicase proteins together with enhanced green fluorescent protein (EGFP, quantum yield 0.60) marker gene (BHK-CHIKV-NCT, described by Pohjala *et al.*[26]) was kindly provided by Prof. Andres Merits (University of Tartu, EE). The cell culture media, the supplements, and other reagents were purchased from Gibco® Life Technologies Corp. (Paisley, UK) and from Sigma Aldrich.

B. Ormocomp® microfabrication by single-step UV lithography

Ormocomp® microchannels of varying nominal widths (10–200 μm) were patterned on top of glass substrates (Pyrex glass, thickness 350 μm) that were dehydrated in an oven at +120 °C for 1 h (Fig. 1). The first planar (base) layer of Ormocomp® (15 μm) was spincoated on top of the glass substrate at 6000 rpm for 30 s and flood exposed on a MA-6 mask aligner (SÜS MicroTec Inc., Germany) using a UV dose of 76 mJ/cm^2 [Figs. 1(a) and 1(b)]. No softbake was applied before UV exposure of the base layer or of the subsequent channel layer. After UV exposure, post-exposure bake was done on a hotplate at +95 °C for 5 min. The second (channel) layer of Ormocomp® was spincoated on top of the first layer at 6000, 2000, or 1400 rpm for

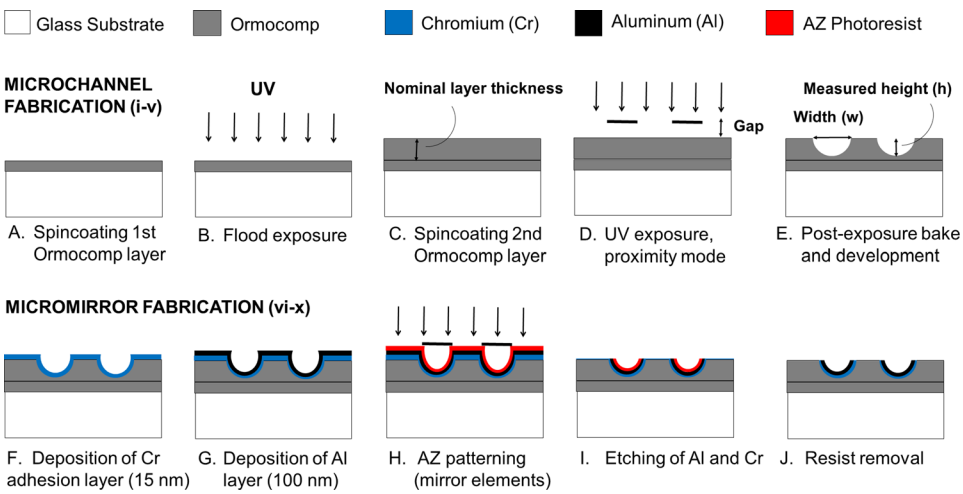

FIG. 1. Schematic presentation of the microfabrication workflows for implementing round cross-sectional shape on Ormocomp® microchannels (a)–(e) and for patterning parabolic Al mirror elements (2×2 mm^2) on top of Ormocomp® microchannels (f)–(j). The nominal microchannel width (w, step E) is the linewidth on the photomask. The proximity gap (step D), which is one of the variables, is the distance between the photomask and the topmost Ormocomp® layer.

30 s to yield 15-, 35-, or 45-μm-thick Ormocomp® layers, respectively [Fig. 1(c)]. The microchannels were patterned on the second layer by varying the UV exposure dose (13, 19, 29, or 48 mJ/cm^2) and the proximity gap (400, 500, 600, 700, 900, or 1000 μm), after which post-exposure bake was done on a hot plate at +95 °C for 5 min [Fig. 1(d)]. The microchannels were developed in an OrmoDEV® developer for 5 min, rinsed with isopropanol, and dried with nitrogen gas [Fig. 1(e)]. The critical fabrication parameters are summarized in Table I. The aluminum (Al) elements of 2×2 mm^2 were patterned on top of parabolic Ormocomp® channels to serve as micromirrors. A chromium (Cr, thickness 15 nm) adhesion layer and an Al layer (100 nm) were sputtered sequentially [Figs. 1(f) and 1(g)] and patterned by using an AZ4562 photoresist, followed by resist development in the AZ351 B developer for 90 min and etching of Al (10 s, 56 °C) and Cr (7 s, room temperature) in their respective etchants [Figs. 1(h) and 1(i)]. Following resist removal in an AZ100 remover for 5–8 min [Fig. 1(j)], the microchannels were rinsed with isopropanol and dried with nitrogen gas.

C. Characterization of Ormocomp® microstructures

The effects of UV exposure conditions (exposure dose and proximity gap) on the microchannel height (h) were determined from three replicate samples of each type (varying microchannel widths and nominal layer thicknesses) by using a Dektak/XT profilometer (Bruker Inc, Karlsruhe, Germany) with 15 mg stylus force and a scan resolution of 0.02 μm.

The effects of UV exposure conditions on the microchannel cross-sectional shape were determined from three replicate samples of each type by using a scanning electron microscope (SEM EBL Zeiss Supra 40, Oberkochen, Germany). Before SEM analysis, a 20 nm chromium (Cr) layer was sputtered on Ormocomp® and the microchannels were diced using a dicing saw. The SEM images were analyzed with Matlab as described in the supplementary material (Fig. S-1), to determine the radius of curvature (r) of the microchannel cross-sections. The Matlab calculations were repeated six times for each image and the results were averaged to eliminate the error due to image processing. In addition, three independent images were analyzed to calculate the variance (due to microfabrication) between three different samples of each type.

D. Characterization of micromirrors by epifluorescence microscopy

For fluorescence measurements, the Ormocomp® microchannels incorporating the Al micromirrors were sealed with a PDMS layer prepared by mixing the elastomer and the curing agent in a ratio of 9:1 (w/w) and cured in the oven at +70 °C overnight. The efficiency of signal enhancement due to the mirror elements was determined by epifluorescence microscopy using a Zeiss AxioScope A1 upright microscope (Carl Zeiss Oy, Espoo, Finland) equipped with a 100 W halogen lamp as the fluorescence excitation source. The fluorescence emission was collected between 500 and 700 nm using an excitation filter of 488 ± 5 nm and Plan Neofluar objectives 10×/0.30 or 20×/0.4 Corr (Carl Zeiss). The fluorescence emission was quantified using a Hamamatsu R5929 photomultiplier tube connected to the microscope and equipped with integrated housing and signal amplifier modules (Cairn Research, Faversham, UK). The background recorded on top of the mirror element and next to the mirror element (no mirror) was subtracted from the fluorescence emissions recorded for 1 μM fluorescein solution or for

TABLE I. Summary of the critical fabrication parameters: The nominal thicknesses of the Ormocomp® base and channel layers with the corresponding spinning speeds and the UV exposure doses and proximity gap distances used in the study.

Layer	Nominal thickness (μm)	Spinning speed (rpm)	UV exposure dose (mJ/cm^2)	Proximity gap distance (μm)
Base	15	6000	76	400
Channel	15	6000	13, 19, 29, or 48	400, 500, 600, 700, 900, or 1000
	35	2000		
	45	1400		

single cells expressing EGFP, and the signal enhancement ratios were calculated of the signal intensities obtained with and without the mirror. The fluorescence micrographs (cell imaging) were recorded with a Moticam 5000 CCD digital color microscope camera (Motic, Xiamen, China) using an exposure time of 5.7 s.

E. Cell culturing

BHK-CHIKV-NCT cells were cultured in Dulbecco's Modified Eagle's Medium with 4.5 g/l glucose, 580 μg/ml L-glutamine, and 25 mM HEPES, supplemented with 7.5% fetal bovine serum, 2% tryptose phosphate broth, 1 mM sodium pyruvate, 100 IU/ml penicillin, 100 μg/ml streptomycin, and 5 μg/ml puromycin, and incubated at 37 °C, 5% CO_2, and 95% humidity. For fluorescence imaging, the cells were detached from the culture flask with trypsin and resuspended into culture media to yield a concentration of 1×10^6 cells/ml.

III. RESULTS AND DISCUSSION

A. Fabrication of Ormocomp® microchannels with round cross-sectional shape

1. Effect of the UV exposure dose

In this work, the formation of the residual layer upon over exposure of Ormocomp® in the proximity mode was exploited to implement microchannels with a round cross-sectional shape in a controlled manner. The effect of UV exposure dose (13, 19, 29, or 48 mJ/cm^2) on the channel cross-sectional shape was first determined as a function of the nominal microchannel width using a fixed layer thickness of 35 μm and a constant proximity gap of 400 μm. Under these conditions, we obtained a round (concave) cross-sectional profile with a tunable radius of curvature (r) for microchannels between 20 and 100 μm in width. The effect of the microchannel nominal width on the steepness of the cross-sectional profile is illustrated in Fig. 2. However, for channel widths <30 μm, the round cross-sectional shape was effectively reproduced only at low UV doses ≤ 19 mJ/cm^2, whereas higher UV doses resulted in almost complete filling of the microchannel by the residual layer (see Fig. S-2 in the supplementary material). For channel widths >100 μm, the parabolic cross-sectional shape was only reproduced at the highest UV dose tested (48 mJ/cm^2), whereas lower UV doses resulted in vertical-walled microchannels with flat bottom (see Fig. S-2 in the supplementary material). It was concluded that as the exposure dose increases, the residual layer becomes thicker, reducing the channel height (h) and increasing r. The evolutions of r and h as a function of

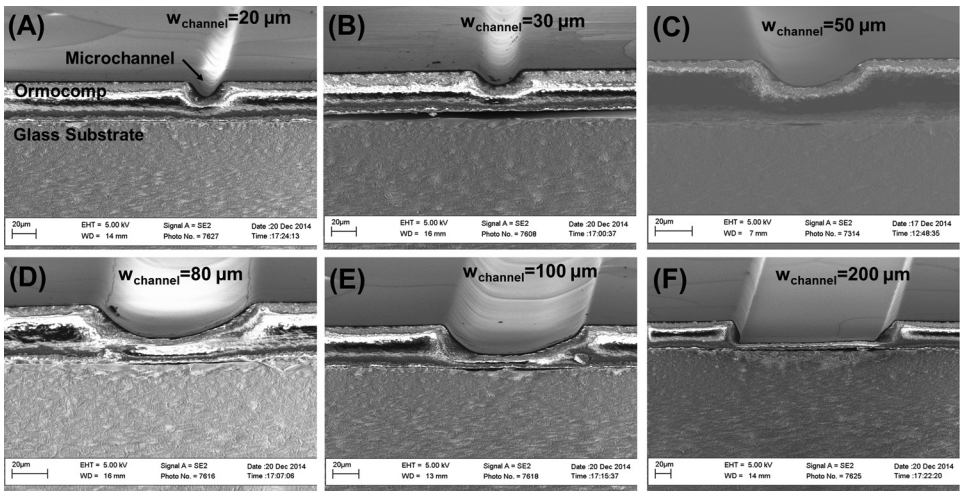

FIG. 2. SEM images illustrating the evolution of the radius of curvature (r) as a function of the microchannel nominal width. In all cases, the nominal Ormocomp® layer thickness was 35 μm, the UV exposure dose was 19 mJ/cm^2, and the proximity gap during UV exposure was 400 μm.

increasing UV exposure dose are given in Figs. 3(a) and 3(b), respectively. For the channel widths between 50 and 100 μm, the increase in r between the lowest and the highest exposure doses was approximately twofold or more. We propose that the mechanism is related to diffraction of light in the proximity (noncontact) exposure mode which results in curved sidewalls and a concave cross-sectional profile of Ormocomp® microchannels (as illustrated in Fig. 3). Thus, such cross-sectional shape is unique to Ormocomp® as it differs from the negatively sloped t-topped profiles commonly observed with other negative photoresists, such as SU-8.[25,27] However, *via* overexposure from backside, SU-8 lithography may also result in tilted, V-shaped sidewalls[27] similar to those observed in Fig. 2(f), but not likely in round-shaped (concave) cross-sectional profiles.

2. Effect of the proximity gap

The effect of proximity gap (see step iv in Fig. 1) on the channel cross-sectional shape was also determined as a function of the nominal microchannel width using a fixed layer thickness of 35 μm and gap distances of 400, 500, 600, 700, 900, or 1000 μm. A constant UV exposure dose of 19 mJ/cm^2, which reproduced the parabolic shape also in narrower channels, was applied in all cases. It was observed that the microchannel height (h) decreased linearly (R^2 between 0.9788 and 0.9999 for all microchannel widths) as a function of gap distance from 400 μm to 600 μm [Fig. 3(c)], indicating a linear increase in the residual layer thickness within this range. A similar effect (evolution of round, concave cross-sectional shape) is thus obtained by tuning the gap (constant UV exposure dose) as by tuning the UV exposure dose (constant gap distance). The narrower the nominal channel width, the sooner (at smaller gap distances) the residual layer thickness reached a saturation point in terms of the microchannel height. At the greatest gap distances, the narrowest microchannels ($w < 30$ μm) were already completely filled with the residual layer, following the trend illustrated in the supplementary material (Fig. S-2).

3. Effect of the microchannel aspect ratio

The effect of the microchannel aspect ratio on the channel cross-sectional shape (r and h) was further explored as a function of the microchannel aspect ratio by varying both the nominal layer thickness (15, 35, or 45 μm) and the nominal microchannel width. A constant UV exposure dose of 19 mJ/cm^2 or 28 mJ/cm^2 and a proximity gap of 400 μm were applied in all cases. It was observed that the radius of curvature (r) was inversely proportional to the aspect ratio with linear regression ($R^2 = 0.9857$ for 19 mJ/cm^2 and and $R^2 = 0.9958$ for 28 mJ/cm^2) within the aspect ratio range of 0.2–0.4 [Fig. 4(a)]. In other words, narrow and deep channels (higher aspect ratio) provided steeper and parabolic cross-sectional profiles, whereas shallow and wide channels (lower aspect ratio) result in milder slopes closer to a circular arc [Fig. 4(b)]. Thus, by considering the aspect ratio (microchannel width and nominal layer thickness) in addition to the UV exposure dose and the distance proximity gap, it is possible to tune the radius of curvature in a wide range toward nearly any desired shape.

4. Error analysis

Two types of variances were considered in order to evaluate the reliability of the Matlab based image analysis used for the determination of the radius of curvature (r) from the SEM images. First, to determine the reproducibility of manual point picking, which was the basis for the image analysis (see supplementary material), each image was independently analyzed six times. At best, the standard error of repeated analysis ($n = 6$) of a single image was down to 2.8% of the mean. However, the variability in the viewing angle (tilt) of the SEM images also affected the repeatability of the image analysis with higher standard error characteristic for images with greater tilt. As a result, the standard errors of the individual image analyses were between 3.0% and 13.4% of the mean ($n = 6$), whenever the round cross-sectional shape was reproduced at appropriate combinations of UV exposure time, gap distance, and aspect ratio. For very narrow channels completely filled with the residual layer and for wide channels

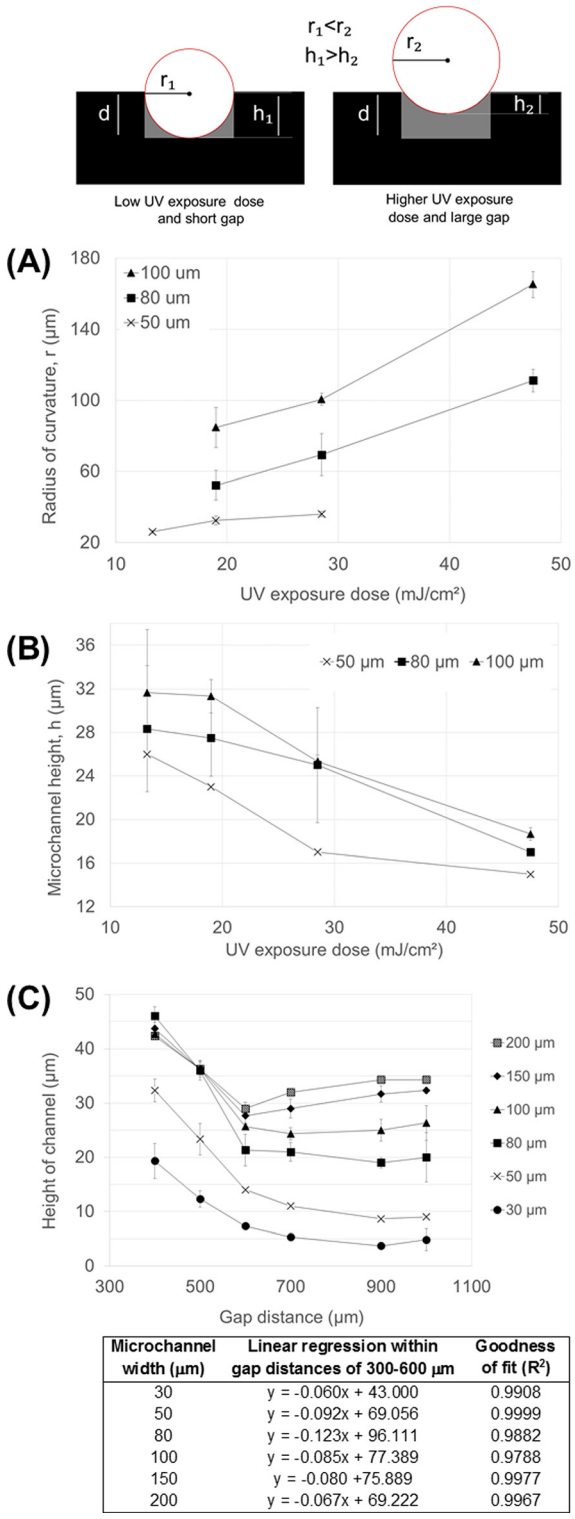

Microchannel width (μm)	Linear regression within gap distances of 300-600 μm	Goodness of fit (R^2)
30	y = -0.060x + 43.000	0.9908
50	y = -0.092x + 69.056	0.9999
80	y = -0.123x + 96.111	0.9882
100	y = -0.085x + 77.389	0.9788
150	y = -0.080 +75.889	0.9977
200	y = -0.067x + 69.222	0.9967

FIG. 3. Illustration of the effects of the UV curing dose and the proximity gap on the microchannel radius of curvature (r) and height (h). Symbol d denotes the nominal thickness of the microchannel layer. The difference between the nominal thickness (d) and the measured height (h) is the residual layer thickness. (a) The microchannel radius of curvature (r) and (b) the microchannel height (h) as a function UV exposure dose. In all cases, Ormocomp® layer thickness was 35 μm, and the proximity gap during exposure was 400 μm. (c) The microchannel height (h) as a function of the distance of the proximity gap with linear regression analyses between gap distances 400 and 600 μm. The Ormocomp® layer thickness was 35 μm and the UV exposure dose was 19 mJ/cm^2.

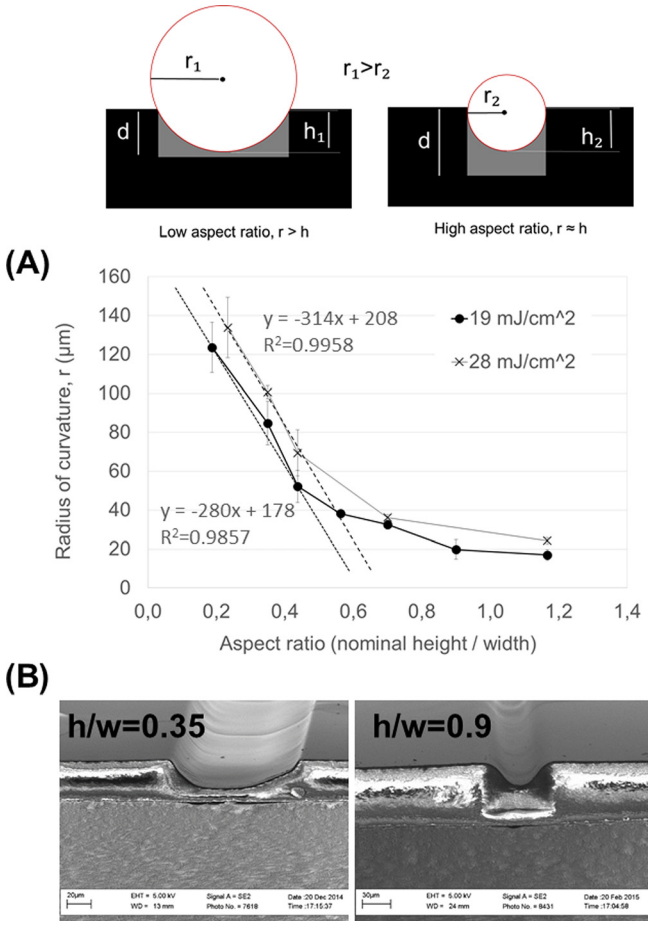

FIG. 4. Illustration of the effect of the microchannel aspect ratio (h/w) on the microchannel radius of curvature (r). Symbol d denotes the nominal thickness of the microchannel layer. The difference between the nominal thickness (d) and the measured height (h) is the residual layer thickness. (a) The microchannel radius of curvature (r) as a function of aspect ratio under a constant UV exposure dose of 19 mJ/cm^2 or 29 mJ/cm^2 and a proximity gap of 400 μm. (b) SEM images of the cross-sectional shapes produced with aspect ratios of 0.35 (nominal channel width 100 μm and layer thickness 35 μm) and 0.9 (nominal channel width 50 μm and layer thickness 45 μm).

featuring very mild slope (or vertical walls with flat bottom), the standard error was typically between 15 and 30% of the mean, and thus these were excluded from the data interpretation. To determine the repeatability of the microfabrication process, we analyzed SEM images of three independent channels with the same fabrication parameters and calculated the standard error of the mean values (of six repeated image analyses) obtained for each of the three images/samples. The standard error describing the repeatability of microfabrication was between 0.8 and 8.3% of the mean ($n = 3$ of each channel type). Again, greater deviation (standard error of 11%–21% of the mean) was observed for wide channels when the UV exposure conditions produced a barely rounded shape.

B. Concave micromirrors in single cell imaging

The possibility to tune the microchannel cross-sectional shape in a controlled manner provides interesting new approaches and great flexibility to the microsystem design. Although under certain conditions, the photolithography of common negative photoresists (e.g., SU-8) may result in tilted sidewalls,[25,27] to our knowledge, the lithography-based patterning of Ormocomp®, as demonstrated in this work, is the sole method capable of reproducing parallel round (concave) shapes of different radius of curvature on the same wafer at high speed (few

seconds) *via* single step lithography. However, by using Ormocomp® microstructures as masters, the same shapes can be easily reproduced on other UV and heat curable polymers as demonstrated in the supplementary material (Fig. S-3).

In this work, the round microchannel cross-sectional profile was used to produce concave micromirrors of different radii of curvature, and thus of different focal lengths, on Ormocomp®. Aluminum (Al) was chosen as the mirror material owing to its high reflectivity (>90%) in the UV and visible ranges. Al thin-film elements were patterned on top of the Ormocomp® channels as described in Fig. 1 (steps F-J), after which the channels were sealed with a gas-permeable PDMS layer [Figs. 5(a) and 5(b)]. The feasibility of the micromirrors for single cell imaging was then examined by upright epifluorescence microscopy.

The signal enhancement ratio was first determined using a 1 μM fluorescein solution. As the results of the reflection of the excitation beam and the improved collection of the emitted fluorescence beam (thanks to focusing), the concave mirror elements provided up to 8-fold higher gain compared with the signal recorded through the uncoated, round Ormocomp® channel [Fig. 5(d)]. The signal enhancement ratio reached the maximum when the focal length of the micromirror was equal to the microchannel height, as in the 80- and 100-μm-wide channels [Figs. 5(c) and 5(d)]. These microchannel widths also provided statistically significant (p values 0.036 and 0.0013, respectively) improvement in signal enhancement ratio compared with the flat-bottomed channels (200 μm in width). In a prior study, a similar 8-fold increase in the fluorescence signal was reached by combining planar silver mirror elements (deposited on a flat-bottomed PDMS channel) with polymer microlens arrays (fabricated *via* thermal reflow of positive photoresist AZ9260).[28] Integration of the microlens array, however, required careful alignment of the lenses with the micromirrors (microchannels), whereas in this work, the 8-fold increase was reached by using the concave micromirrors alone, without the need for prior focusing of the excitation beam (by a microlens) and, thus, at ease without particular alignment issues. Moreover, thanks to the uniformity of the aluminum reflectance over a wide wavelength

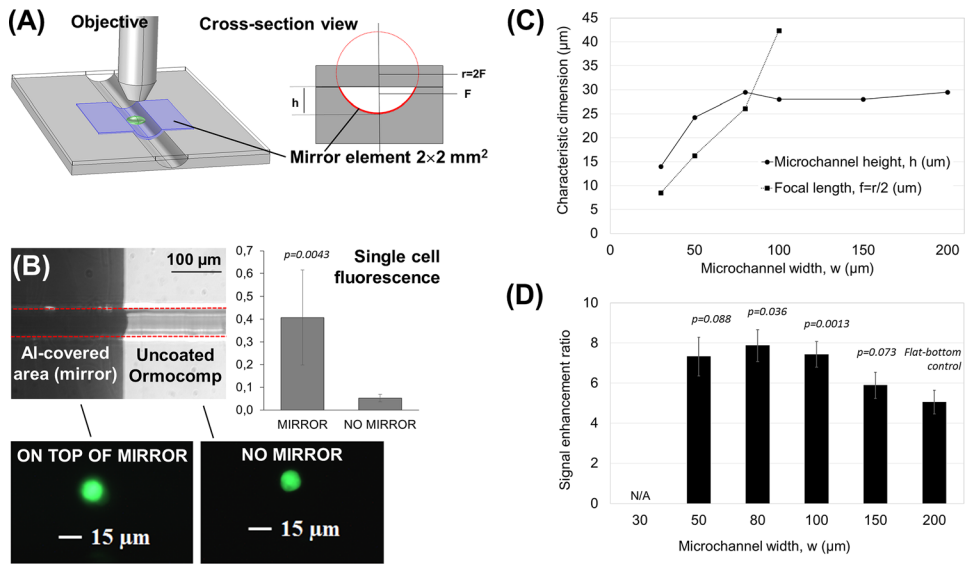

FIG. 5. Ormocomp® microfluidic channels with concave micromirrors for optical signal enhancement in epifluorescence microscopy. (a) Schematic 3D view and a cross-sectional view of the setup used in micromirror experiments. h = microchannel height, r = radius of curvature, and F = focal point. (b) An optical micrograph of a 80-μm-wide Ormocomp® microchannel with mirror element illustrating the round cross-sectional shape, and comparison of the single cells' fluorescence together with fluorescent micrographs obtained of single cells under constant exposure conditions through the uncoated, round Ormocomp® channel (no mirror) and on top of the mirror element. (c) Measured microchannel heights (h) and micromirror focal lengths (f) and (d) the signal enhancement ratios obtained in curved microchannels (for 1 μM fluorescein) as a function of the microchannel width, with p values indicating their statistical significance compared with the flat-bottom control (i.e., the 200-μm-wide channel). The nominal microchannel layer thickness was 35 μm, the UV exposure dose was 19 mJ/cm^2, and the proximity gap was 400 μm.

region, ranging from ca. 200 nm to 500 nm, similar signal enhancement can be expected for any fluorescent dye, which exhibits excitation and emission maxima in this range. It is also likely that comparable signal enhancement ratios are reached if similar tilted sidewalls or concave profiles are patterned, for instance, *via* overexposure of SU-8 from backside[27] or *via* replication of the round-shape onto other UV-curable polymers, such as thiol-enes (Fig. S-3), respectively.

Next, the signal enhancement ratio was determined for single EGFP expressing cells loaded into the Ormocomp® microchannel as a suspension of 1×10^6/ml in the cell culture medium. The fluorescence of individual cells was recorded on top of the micromirror and compared to that obtained through the uncoated, round Ormocomp® channel (next to the mirror). The signals obtained on top of the mirror and through the uncoated, round channel were 0.41 ± 0.21 a.u. ($n = 6$ cells) and 0.05 ± 0.01 a.u. ($n = 5$ cells), respectively, thus resulting in a statistically significant ($p = 0.0043$) enhancement ratio of 7.8 [Fig. 5(b)], similar to the fluorescein solution. The signal enhancement on top of the mirror element was also easily observed by the naked eye, as illustrated with single cells' fluorescence in Fig. 5(b). In addition to the improved detection sensitivity, concave micromirrors can also be used to obtain a magnified image of the cell and thus to improve the spatial resolution of single cell imaging. In this case, however, the object (i.e., the single cell) needs to be between the focal point (F) and the center of radius (2F). In other words, to improve the spatial resolution, the micromirror focal length (f) needs to be smaller than the microchannel height (h) [Fig. 5(c)]. Conveniently, the lithographic processing of Ormocomp® also allows fabrication of such mirror structures at ease. Moreover, Ormocomp® is inherently biocompatible and thus directly feasible for a variety of cell-based applications, ranging from cell culturing[15,16] to cell migration assays.[17] For instance, Ormocomp® has been shown to promote the adherence and maturation of retinal pigment epithelial cells (derived from human embryonic stem cells), better than other common glass silanization processes.[16] The possibility to adhesively bond the Ormocomp® channels with a gas permeable and transparent PDMS layer further improves the feasibility of Ormocomp® devices for live-cell imaging by facilitating efficient oxygen diffusion through the cover layer. Finally, by implementing concave micromirrors at the bottom of Ormocomp® channels, it is possible to significantly improve both the sensitivity and the spatial resolution of (single) cell imaging.

IV. CONCLUSIONS

This work describes controlled fabrication of Ormocomp® microchannels with round cross sectional shapes of tunable radii of curvature, and the implementation of concave micromirrors of tunable focal length by patterning Al thin-film elements on top of the Ormocomp® channels. The fabrication process relies on controlled overexposure of Ormocomp® during a single step optical lithography, which allows one to adjust the radius of curvature simply by varying the exposure dose or the distance of the proximity gap. Together with the nominal width and depth (layer thickness) of the microchannel, these parameters determine the radius of curvature. By increasing the UV exposure dose or the proximity gap, the radii of curvature increased and changed the shape of the cross-sectional profile from steep, parabolic shape to a wide, spherical (circle-arc) shape. Thus, by controlling the exposure dose or gap distance, different radii of curvature could be obtained for the same feature width. On the other hand, at constant exposure conditions, the steepness of the curvature increased as a function of increasing microchannel aspect ratio. In summary, by exploiting the residual layer formation of Ormocomp® during single step lithography, it is possible to vary the microchannel cross-sectional shape (radius of the curvature) in a wider range than that feasible for other existing microfabrication materials and methods (e.g., isotropic etching of glass). By using Ormocomp® microstructures as masters, replication of the round shape on other UV or heat curable polymers is also feasible *via* PDMS soft lithography. Most importantly, the inherent high surface smoothness resulting from lithographic patterning of Ormocomp® enables straightforward implementation of concave micromirrors of high optical quality and tunable focal length as integral parts of the Ormocomp® microfluidic devices. Up to 8-fold signal enhancement in single cell imaging by epifluorescence microscopy was demonstrated in this work with the help of the concave micromirrors. Together

with the inherent good biocompatibility of Ormocomp®, the approach reported herein thus provides flexible grounds for fabrication of bioanalytical and biomedical microdevices.

SUPPLEMENTARY MATERIAL

See supplementary material for descriptions of the image analysis by using custom-made Matlab code, of the effects of UV exposure conditions on the microchannel cross-sectional shape, and of the replication of the round cross-sectional shape on other materials.

ACKNOWLEDGMENTS

The research leading to these results has received funding from the European Research Council under the European Union's Seventh Framework Program (FP/2007–2013)/ERC Grant Agreement No. 311705. Financial support for the work was also provided by the Academy of Finland (Grant Nos. 266820 and 297360) and the University of Helsinki Research Funds. We also thank the Micronova Nanofabrication Centre, Aalto University, for providing access to the cleanroom facilities, and the Drug Discovery and Chemical Biology Network, for providing support for cell-based experiments.

APPENDIX: MATLAB CODE FOR IMAGE ANALYSIS

Matlab script: circ.m
Matlab script: pickpoint.m

[1]O. Solgaard, A. A. Godil, R. T. Howe, L. P. Lee, Y. A. Peter, and H. Zappe, J. Microelectromech. Syst. **23**, 517 (2014).
[2]S. Franssila, *Introduction to Microfabrication*, 2nd ed. (John Wiley & Sons Ltd, West Sussex, 2010).
[3]G. J. Wang, K. H. Ho, S. H. Hsu, and K. P. Wang, Biomed. Microdevices **9**, 657 (2007).
[4]J. Y. Kim, K. Pfeiffer, A. Voigt, G. Gruetznerb, and J. Brugger, J. Mater. Chem. **22**, 3053 (2012).
[5]B. Bao, J. Jiang, F. Li, P. Zhang, S. Chen, Q. Yang, S. Wang, B. Su, L. Jiang, and Y. Song, Adv. Funct. Mater. **25**, 3286 (2015).
[6]R. Pericet-Camera, A. Best, S. K. Nett, J. S. Gutman, and E. Bonaccurso, Opt. Express **15**, 9877 (2007).
[7]C. M. B. Ho, S. H. Ng, K. H. H. Li, and Y. J. Yoon, Lab Chip **15**, 3627 (2015).
[8]B. C. Gross, J. L. Erkal, S. Y. Lockwood, C. Chen, and D. M. Spence, Anal. Chem. **86**, 3240 (2014).
[9]C. Schizas and D. Karalekas, J. Mech. Behav. Biomed. Mater. **4**, 99 (2011).
[10]S. Aura, T. Sikanen, T. Kotiaho, and S. Franssila, Sens. Actuators, B **132**, 397 (2008).
[11]A. Singh, G. Scotti, T. Sikanen, V. Jokinen, and S. Franssila, Micromachines **5**, 472 (2014).
[12]L. Jacot-Descombes, V. J. Cadarso, A. Schleunitz, S. Grützner, J. J. Klein, J. Brugger, H. Schift, and G. Grützner, Opt. Express **23**, 25365 (2015).
[13]T. Sikanen, S. Aura, L. Heikkilä, T. Kotiaho, S. Franssila, and R. Kostiainen, Anal. Chem. **82**, 3874 (2010).
[14]T. Sikanen, S. Aura, S. Franssila, T. Kotiaho, and R. Kostiainen, Anal. Chim. Acta **711**, 69 (2012).
[15]F. Klein, B. Richter, T. Striebel, C. M. Franz, G. von Freymann, M. Wegener, and M. Bastmeyer, Adv. Mater. **23**, 1341 (2011).
[16]E. Käpylä, A. Sorkio, S. Teymouri, K. Lahtonen, L. Vuori, M. Valden, H. Skottman, M. Kellomäki, and K. Juuti-Uusitalo, Langmuir **30**, 14555 (2014).
[17]S. H. Yoon, Y. K. Kim, E. D. Han, Y. H. Seo, B. H. Kim, and M. R. K. Mofrad, Lab Chip **12**, 2391 (2012).
[18]A. Ovsianikov, S. Schlie, A. Ngezahayo, A. Haverich, and B. N. Chichkov, J. Tissue Eng. Regener. Med. **1**, 443 (2007).
[19]S. H. Mahmoud, A. E. El-Embaby, and A. M. AbdAllah, Oper. Dent. **39**, 32 (2014).
[20]K. H. Haas, S. Amberg-Schwab, and K. Rose, Thin Solid Films **351**, 198 (1999).
[21]R. Houbertz, L. Fröhlich, M. Popall, U. Streppel, P. Dannberg, A. Bräuer, J. Serbin, and B. N. Chichkov, Adv. Eng. Mater. **5**, 551 (2003).
[22]S. Aura, V. Jokinen, S. Franssila, M. Laitinen, and T. Sajavaara, J. Micromech. Microeng. **21**, 125003 (2011).
[23]V. Jokinen, S. Aura, L. Luosujärvi, L. Sainiemi, T. Kotiaho, S. Franssila, and M. Baumann, J. Am. Soc. Mass Spectrom. **20**, 1723 (2009).
[24]S. Aura, V. Jokinen, L. Sainiemi, M. Baumann, and S. Franssila, J. Nanosci. Nanotechnol. **9**, 6710 (2009).
[25]R. Daunton, A. J. Gallant, and D. Wood, J. Micromech. Microeng. **22**, 075016 (2012).
[26]L. Pohjala, A. Utt, M. Varjak, A. Lulla, A. Merits, T. Ahola, and P. Tammela, PLoS One **6**, e28923 (2011).
[27]Y. J. Chang, K. Mohseni, and V. M. Bright, Sens. Actuators, A **136**, 546 (2007).
[28]J. Lim, P. Gruner, M. Konrad, and J. C. Baret, Lab Chip **13**, 1472 (2013).